Electromagnetic backscattering from one-dimensional drifting fractal sea surface II: Electromagnetic backscattering model*

Tao Xie(谢涛)[1,2,†], William Perrie[3], Shang-Zhuo Zhao(赵尚卓)[1,2], He Fang(方贺)[1,2], Wen-Jin Yu(于文金)[1,2], and Yi-Jun He(何宜军)[1,2]

[1] School of Marine Sciences, Nanjing University of Information Science and Technology, Nanjing 210044, China
[2] Jiangsu Engineering Technology Research Center of Marine Environment Detection, Nanjing 210044, China
[3] Bedford Institute of Oceanography, B2Y 4A2, Dartmouth, NS, Canada

(Received 20 October 2015; revised manuscript received 12 January 2016; published online 1 June 2016)

Sea surface current has a significant influence on electromagnetic (EM) backscattering signals and may constitute a dominant synthetic aperture radar (SAR) imaging mechanism. An effective EM backscattering model for a one-dimensional drifting fractal sea surface is presented in this paper. This model is used to simulate EM backscattering signals from the drifting sea surface. Numerical results show that ocean currents have a significant influence on EM backscattering signals from the sea surface. The normalized radar cross section (NRCS) discrepancies between the model for a coupled wave-current fractal sea surface and the model for an uncoupled fractal sea surface increase with the increase of incidence angle, as well as with increasing ocean currents. Ocean currents that are parallel to the direction of the wave can weaken the EM backscattering signal intensity, while the EM backscattering signal is intensified by ocean currents propagating oppositely to the wave direction. The model presented in this paper can be used to study the SAR imaging mechanism for a drifting sea surface.

Keywords: fractal, ocean current, electromagnetic scattering, normalized radar cross section (NRCS)

PACS: 41.20.Jb, 84.40.Xb, 91.50.Iv, 92.10.Hm **DOI:** 10.1088/1674-1056/25/7/074102

1. Introduction

Currents have significant effects on the environment, whether in nearshore areas or in the deep sea ocean, because currents can diffuse pollutants such as crude oil spills, drifting marine debris, red tide outbreaks, and related variables. Military applications and knowledge of ocean currents are key factors in successful naval operations, especially for amphibious programs, countermeasures for mines or terrorism, deepwater submarine voyages, and other special operations.[1]

Currents can be directly measured by the acoustic Doppler current profiler (ADCP) and moorings. However, these direct measurement methods cannot meet the requirements for large-scale, quasi real-time and synchronous measurements.[2] To meet these needs, attention has been focused on indirect measurements of currents, i.e., remote sensing technology.

High-frequency (HF) radar is the most prevalent ground-based remote sensing system for measuring currents. HF radar data are used to model oil spills, for maritime search and rescue operations, assimilation in numerical circulation models and relevant activities.[3–9] Because the HF radar wavelength is relatively large (10–100 m), its antenna scale determines the extent to which HF radar can measure the currents of the coastal waters (100–300 km from land area).

To reduce the limitations of HF radar, satellite or airborne visible and infrared imaging sensors have been developed to measure ocean wave velocity and surface currents. Satellite and airborne sensors have the advantages of good maneuverability, wide measuring range, and short revisit periods. By exploiting the temporal lag between the panchromatic and multispectral scenes, the phase velocity fields of ocean waves can be derived from space-borne optical images from the SPOT-5.[10] Surface currents can also be retrieved from airborne visible image time series. Temporal sequences of optical and infrared images can be used to retrieve current velocities by tracking modulations in the radiance from the surface.[1,2,11,12] The dominant mechanism is based on the full three-dimensional (3D) frequency–wavenumber spectrum of the luminance modulations, which exhibits the dispersion relation for surface gravity waves.

Using temporal sequences of optical and infrared images obtained from airborne and satellite imaging, current retrieving methods can overcome some of the defects of HF radar capacity to measure currents. However, a limitation that op-

*Project supported by the National Natural Science Foundation of China (Grant No. 41276187), the Global Change Research Program of China (Grant No. 2015CB953901), the Priority Academic Program Development of Jiangsu Higher Education Institutions, China, the Program for the Innovation Research and Entrepreneurship Team in Jiangsu Province, China, the Canadian Program on Energy Research and Development, and the Canadian World Class Tanker Safety Service Program.

†Corresponding author. E-mail: xietao@nuist.edu.cn

© 2016 Chinese Physical Society and IOP Publishing Ltd

tical and infrared sensors cannot capture ocean surface measurements in cloudy weather still exists because optical and infrared sensors cannot penetrate through clouds. It is therefore necessary to use microwave remote sensing technology to detect surface currents. Synthetic aperture radar (SAR) is potentially a promising remote sensor of currents. The feasibility of measuring ocean currents using SAR data was first presented in 1979.[13] This method exploits the Doppler centroid anomalies of conventional SAR raw data to retrieve the currents.[4–16] Another SAR technology for current retrievals was presented and known as along track interferometry (ATI) technology.[17–19] The ATI is based on the interferometric combination of two complex SAR images of the same scene. There is a short lag, of the order of milliseconds, between these two images. The Doppler shift of the backscattered signal is linked to the phase discrepancy between the two images. Theoretically, the ATI can retrieve currents in every SAR pixel, while the Doppler centroid anomaly analysis can reduce the SAR resolution. Thus, there is no significant difference in the actual result between the two techniques. The key defect of these two techniques is that a stationary reference point, such as land, is required to appear in the SAR image. Therefore, microwave remote sensing of surface current has been still in the exploration stage so far.

Our purpose is to study the modulation characteristics of surface currents on electromagnetic (EM) backscattering signals. A one-dimensional (1D) fractal sea surface wave–current model has been derived based on the mechanism of wave–current interaction in Part 1[20] of this work. In the present study, based on the coupled wave–current model presented in Part 1, an electromagnetic backscattering model of wave–current interactions at the sea surface is derived in Section 2. The numerical results of electromagnetic backscattering are given in Section 3. Conclusions are drawn from the present study in Section 4.

2. Electromagnetic backscattering model of wave–current coupled sea surface

Based on a 1D fractal sea surface ocean wave–current model presented in Part 1,[20] the electromagnetic backscattering model of wave–current coupled sea surface is derived as follows.

According to Part 1,[20] the 1D wave–current linear fractal sea surface is

$$y' = f(x',t) = \sum_{n=0}^{N-1} \sigma C b^{(s-2)n} \left(1-\frac{k_0 b^n}{\omega_n} C_0\right) \times \sin\left(k_0 b^n x' - \omega_n t + \varphi_n\right), \quad (1)$$

where

$$\omega_n = \sqrt{g k_n} \quad (2)$$

is the dispersion relationship of this model; $k_0 = 2\pi/\lambda_0$ is the dominant ocean wave number, with λ_0 being the dominant wavelength; b $(b>1)$ is the scale factor for amplitude and frequency; σ is the standard deviation of $f(x,t)$ which relates to significant wave height h_s by $\sigma = h_s/4$; $C = \sqrt{\frac{2\left[1-b^{2(s-2)}\right]}{1-b^{2N(s-2)}}}$, with s $(1<s<2)$ being the roughness coefficient of the fractal sea surface. Here, $k_n = k_0 b^n$, ω_n, φ_n are wave number, the radian frequency, and the phase of the n-th wave components, respectively. The dispersion relation for the wave–current coupled dynamics in deep water can be written as $(\omega - kC_0)^2 = kg$, where $g = 9.8\ \mathrm{m\cdot s^{-1}}$ is the acceleration due to gravity.

A schematic of electromagnetic backscattering from the sea surface is shown in Fig. 1. Suppose that the surface current velocity is $C_0\ \mathrm{m\cdot s^{-1}}$. Here, $C_0>0$ when the wave propagates in the x positive direction; $C_0<0$ when the wave propagates in the opposite direction to the x positive direction. The electromagnetic wave interacts with the sea surface with an incidence angle θ_i. k_i is the wave number of the incident wave. k_s is the backscattering wave number. The scattering angle is θ_s $(\theta_s = \theta_i = \theta)$. The relationship between the incident wave number and the backscattering wave number is

$$\boldsymbol{k}_s = -\boldsymbol{k}_i = -k_{em}\sin\theta \boldsymbol{x}_0 + k_{em}\cos\theta \boldsymbol{y}_0, \quad (3)$$

where k_{em} is the electromagnetic wavenumber, $\boldsymbol{x}_0$ and $\boldsymbol{y}_0$ are unit vectors in x and y directions, respectively, and $\boldsymbol{n} = \frac{\boldsymbol{k}_s}{|\boldsymbol{k}_s|} = \frac{-\tan\theta \boldsymbol{x}_0 + \boldsymbol{y}_0}{\sqrt{1+\tan^2\theta}}$ is the unit normal vector of the incident facet.

The far-field scattering problem is considered in this paper. To evaluate the backscattering of the wave–current coupled sea surface with finite conductivity, some initial conditions are simplified. Firstly, the incident wave is assumed to be a plane wave. Secondly, the shadowing effect and multiple scattering are disregarded. Finally, the field of any point of the sea surface can be considered as the sum of the incident field and the scattering fields.

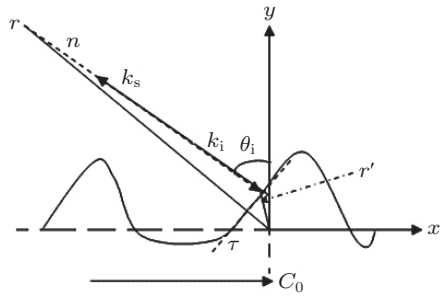


Fig. 1. Schematic of electromagnetic backscattering from sea surface.

The coordinate of the radar observation point in Fig. 1 is $\boldsymbol{r} = (x,y)$, where $|\boldsymbol{r}| = \sqrt{x^2+y^2}$. The EM scattering point is $\boldsymbol{r}' = (\boldsymbol{x}', \boldsymbol{y}')$, where $|\boldsymbol{r}'| = \sqrt{x'^2+y'^2}$. Let the complex dielectric constant of ocean water be ε_1, and the dielectric constant of air be ε_0, then $\varepsilon_r = \varepsilon_1/\varepsilon_0$ will be relative dielectric constant

and generally $\varepsilon_r \gg 1$. Thus, the Fresnel reflection coefficient $R = \frac{\sqrt{\varepsilon_r}-1}{1+\sqrt{\varepsilon_r}}$ can be approximated to be 1. The electric field of the incident wave in a backscattering facet can be written as

$$\boldsymbol{E}_{\mathrm{i}}\left(r'\right) = E_0 \mathrm{e}^{\mathrm{j}\boldsymbol{k}_{\mathrm{i}}\cdot\boldsymbol{r}'}\boldsymbol{q}_{\mathrm{i}}, \tag{4}$$

where E_0 is the magnitude of an electric field vector, and $\boldsymbol{q}_{\mathrm{i}} = \frac{\boldsymbol{k}_{\mathrm{i}}\times\boldsymbol{n}}{|\boldsymbol{k}_{\mathrm{i}}\times\boldsymbol{n}|}$. Then the backscattering electric field of the wave in the facet is

$$\boldsymbol{E}_{\mathrm{s}}\left(r'\right) = E_0 R \mathrm{e}^{\mathrm{j}\boldsymbol{k}_{\mathrm{i}}\cdot\boldsymbol{r}'}\boldsymbol{q}_{\mathrm{i}}. \tag{5}$$

The corresponding magnetic fields of the incident wave and the backscattering wave, respectively, are

$$\boldsymbol{H}_{\mathrm{i}}\left(r'\right) = \left(\boldsymbol{k}_{\mathrm{i}}\times E_0 \mathrm{e}^{\mathrm{j}\boldsymbol{k}_{\mathrm{i}}\cdot\boldsymbol{r}'}\boldsymbol{q}_{\mathrm{i}}\right)/\eta, \tag{6}$$

$$\boldsymbol{H}_{\mathrm{s}}\left(r'\right) = -\left(\boldsymbol{k}_{\mathrm{s}}\times E_0 R \mathrm{e}^{\mathrm{j}\boldsymbol{k}_{\mathrm{i}}\cdot\boldsymbol{r}'}\boldsymbol{q}_{\mathrm{i}}\right)/\eta, \tag{7}$$

where $\eta = \sqrt{\mu_0/\varepsilon_0}$.

According to Huygen's principle,[21] one can obtain an expression for the scattering electric field at $\boldsymbol{r}(\boldsymbol{x},\boldsymbol{y})$ as follows:

$$\begin{aligned}\boldsymbol{E}_{\mathrm{s}}(r) = & \int_{-L}^{L}\left\{\mathrm{j}\omega\mu_0\overline{\overline{G}}\left(\boldsymbol{r},\boldsymbol{r}'\right)\cdot\left[\boldsymbol{n}\times\boldsymbol{H}\left(r'\right)\right]\right.\\ & \left.+\nabla\times\overline{\overline{G}}\left(\boldsymbol{r},\boldsymbol{r}'\right)\cdot\left[\boldsymbol{n}\times\boldsymbol{E}(r')\right]\right\}\mathrm{d}l',\end{aligned} \tag{8}$$

where

$$\boldsymbol{n}\times\boldsymbol{E}\left(r'\right) = (1+R)E_0\mathrm{e}^{\mathrm{j}\boldsymbol{k}_{\mathrm{i}}\cdot\boldsymbol{r}'}(\boldsymbol{n}\times\boldsymbol{q}_{\mathrm{i}}), \tag{9}$$

$$\boldsymbol{n}\times\boldsymbol{H}\left(r'\right) = \frac{E_0}{\eta}\boldsymbol{n}\times\left[(\boldsymbol{k}_{\mathrm{i}}\times\boldsymbol{q}_{\mathrm{i}})+R(\boldsymbol{k}_{\mathrm{s}}\times\boldsymbol{q}_{\mathrm{i}})\right]\mathrm{e}^{\mathrm{j}\boldsymbol{k}_{\mathrm{i}}\cdot\boldsymbol{r}'}, \tag{10}$$

$$\overline{\overline{G}}\left(\boldsymbol{r},\boldsymbol{r}'\right) = \left[\overline{\overline{I}}+\frac{\nabla\nabla}{k_{\mathrm{em}}^2}\right]\cdot\frac{\mathrm{e}^{\mathrm{j}k_{\mathrm{em}}|\boldsymbol{r}-\boldsymbol{r}'|}}{4\pi|\boldsymbol{r}-\boldsymbol{r}'|},$$

with L denoting the fractal sea surface over which the surface integration is to be carried out and $x\in[-L/2,L/2]$. Because the observation point is in the far-field region, the dyadic Green's function can be simplified into

$$\overline{\overline{G}}\left(\boldsymbol{r},\boldsymbol{r}'\right) = \frac{\mathrm{e}^{\mathrm{j}k_{\mathrm{em}}r}}{4\pi r}\mathrm{e}^{-\mathrm{j}k_{\mathrm{em}}r'}\left[\overline{\overline{I}}-k_{\mathrm{s}}k_{\mathrm{s}}\right]. \tag{11}$$

Inserting Eq. (11) into Eq. (8), we have

$$\begin{aligned}\boldsymbol{E}_{\mathrm{s}}(r) = & \frac{\mathrm{j}k_{\mathrm{em}}E_0\mathrm{e}^{\mathrm{j}k_{\mathrm{em}}r}}{4\pi r}\left[\overline{\overline{I}}-k_{\mathrm{s}}k_{\mathrm{s}}\right]\int_{-L}^{L}\left\{\boldsymbol{k}_{\mathrm{s}}\times\left[\boldsymbol{n}\times\boldsymbol{E}(r')\right]\right.\\ & \left.+\eta\left[\boldsymbol{n}\times\boldsymbol{H}(r')\right]\right\}\mathrm{e}^{-\mathrm{j}k_{\mathrm{i}}\cdot r'}\mathrm{d}l'.\end{aligned} \tag{12}$$

Substituting Eqs. (4)–(7), (9), and (10) into Eq. (12), the EM backscattering electric fields can be solved as

$$\begin{aligned}E_{\mathrm{s}}(r) = & \frac{\mathrm{j}k_{\mathrm{em}}\mathrm{e}^{\mathrm{j}k_{\mathrm{em}}r}}{4\pi r}\\ & \times\int_{-L}^{L}\left(2R\cos\theta\,\mathrm{e}^{\mathrm{j}2k_{\mathrm{em}}\left[(\sin\theta)-(\cos\theta)y'\right]}\mathrm{d}x'\right).\end{aligned} \tag{13}$$

Let γ be the scattering coefficient of the sea surface. γ is defined as the ratio between the electric scattering fields $\boldsymbol{E}_{\mathrm{s}}$ and the far-electric field $\boldsymbol{E}_{\mathrm{s0}}$ in the specular direction from a smooth surface with infinite conductibility, i.e.,

$$\gamma = \frac{\boldsymbol{E}_{\mathrm{s}}}{\boldsymbol{E}_{\mathrm{s0}}}. \tag{14}$$

By solving the integral equation (13) for $\boldsymbol{E}_{\mathrm{s0}}$, one can obtain

$$\boldsymbol{E}_{\mathrm{s0}} = j\frac{2k_{\mathrm{em}}L}{4\pi r}\mathrm{e}^{\mathrm{j}k_{\mathrm{em}}r}. \tag{15}$$

By inserting Eqs. (13) and (15) into Eq. (14), the scattering coefficient becomes

$$\gamma = \frac{1}{L\cos\theta}\int_{-L}^{L}\mathrm{e}^{\mathrm{j}2k_{\mathrm{em}}\left[(\sin\theta)-(\cos\theta)y'\right]}\mathrm{d}x'. \tag{16}$$

Substituting Eq. (1) into Eq. (16), we have

$$\begin{aligned}\gamma = & \frac{1}{L\cos\theta}\int_{-L}^{L}\mathrm{e}^{\mathrm{j}2k_{\mathrm{em}}\left[(\sin\theta)-(\cos\theta)y'\right]}\mathrm{d}x'\\ = & \frac{1}{L\cos\theta}\int_{-L}^{L}\tau\left(x',t\right)\mathrm{e}^{\mathrm{j}2k_{\mathrm{em}}\sin\theta}\mathrm{d}x',\end{aligned} \tag{17}$$

where

$$\begin{aligned}&\tau\left(x',t\right)\\ &= \exp\left\{\mathrm{j}\left[\begin{array}{c}-2k_{\mathrm{em}}\cos\theta\sigma C\sum\limits_{n=0}^{N-1}b^{(s-2)n}\\ \left(1-\frac{k_0b^n}{\omega_n}C_0\right)\sin\left(k_0b^nx'-\omega_nt+\varphi_n\right)\end{array}\right]\right\}.\end{aligned} \tag{18}$$

Here, we use cylindrical wave expansion for a planar wave

$$\mathrm{e}^{\mathrm{j}u\sin\zeta} = \sum_{p=-\infty}^{\infty}\mathrm{J}_p(u)\mathrm{e}^{\mathrm{j}p\zeta}. \tag{19}$$

Here, $\zeta\in R$, $\mathrm{J}_p(u)$ is the Bessel function, and $\boldsymbol{p} = (p_0, p_1, p_2, \ldots, p_n, \ldots, p_{N-1})^{\mathrm{T}}$, $p_{\mathrm{n}} = -\infty,\ldots,-2,-1,0,1,2,\ldots,+\infty$. The function $\tau(x',t)$ can be expressed as

$$\begin{aligned}&\tau\left(x',t\right)\\ &= \sum_{p_0,p_1,\ldots,p_n,\ldots,p_{N-1}=-\infty}^{+\infty}\left\{\prod_{n=0}^{N-1}\mathrm{J}_{p_n}\left[-2\sigma k_{\mathrm{em}}Cb^{(s-2)n}\left(1-\frac{k_0b^n}{\omega_n}C_0\right)\cos\theta\right]\right\}\\ &\quad\times\exp\left\{j\left[\sum_{n=0}^{N-1}p_n\left(k_0b^nx'-\omega_nt+\varphi_n\right)\right]\right\}.\end{aligned} \tag{20}$$

One can finally obtain

$$\begin{aligned}\gamma(t) = & \frac{1}{L\cos^2\theta}\sum_{p=-\infty}^{\infty}\prod_{n=0}^{N-1}\mathrm{J}_{p_n}\left[-2\sigma k_{\mathrm{em}}Cb^{(s-2)n}\right.\\ & \left.\times\left(1-\frac{k_0b^n}{\omega_n}C_0\right)\cos\theta\right]\\ & \times\mathrm{sinc}\left[\left(k_{\mathrm{em}}\sin\theta+\frac{1}{2}\sum_{n=0}^{N-1}p_nk_0b^n\right)L\right]\mathrm{e}^{\mathrm{j}p^T\zeta(t)},\end{aligned} \tag{21}$$

where $\zeta(t) = \left[\zeta_0(t),\zeta_1(t),\zeta_2(t),\ldots,\zeta_{N-1}(t)\right]^{\mathrm{T}}$ and $\zeta_n(t) = \varphi_n(t)-\omega_nt$. Equation (21) is the electromagnetic backscattering coefficient of the wave–current coupled fractal sea surface.

3. Numerical results

Based on the scattering coefficient in Eq. (18), one can calculate the normalized radar cross section (NRCS) of the fractal sea surface with the following expression:

$$\sigma_0 = 2\log_{10}\gamma, \tag{22}$$

assuming that RADARSAT-2 SAR is an appropriate remote sensor. The frequencies of its transmitter and receiver are both $f = 5.4$ GHz, and the electromagnetic wavenumber is $k = 2\pi f/v$, where $v = 3\times10^8$ m·s^{-1}. Let $N = 25$, $s = 1.3$, $b = 2e/3$, and dominant wavelength $\lambda_0 = 200$ m, then the dominant wavenumber $k_0 = 2\pi/\lambda_0$. To simulate the sea state with a significant height of 2 m, σ is adopted to be 0.5. The illumination area is $L = 10\lambda_0$. Figure 2 shows the time evolutions of sea surface elevations with different ocean currents. Taking the following case for example: seven ocean current velocities are selected to simulate the fractal sea surface which are shown in Fig. 2.

In Fig. 2, the same waves start with the same phase, and different ocean currents encountered are given in Figs. 2(a)–2(g), where the waves interact with currents. After 337 s, the phases of waves are quite different from each other. Therefore, ocean currents can change ocean wave phases.

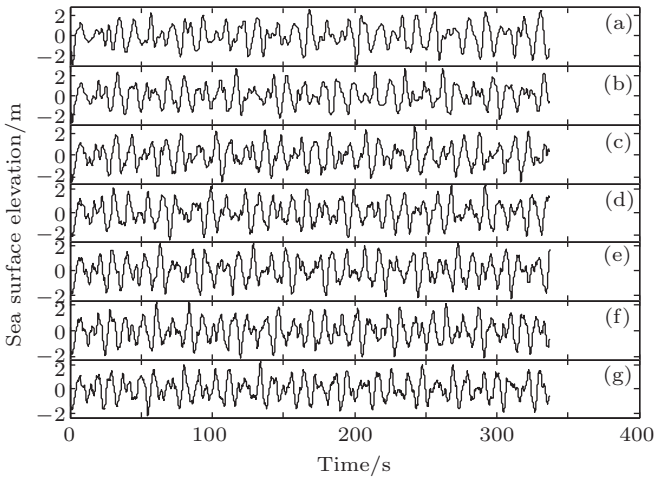


Fig. 2. Time evolutions of sea surface elevation for different ocean current velocities. (a) $C_0 = -1.5$ m·s^{-1}; (b) $C_0 = -1.0$ m·s^{-1}; (c) $C_0 = -0.5$ m·s^{-1}; (d) $C_0 = 0$ m·s^{-1}; (e) $C_0 = 0.5$ m·s^{-1}; (f) $C_0 = 1.0$ m·s^{-1}; (g) $C_0 = 1.5$ m·s^{-1}.

According to Part 1 of this work,[20] the ocean wave spectrum distribution is changed by ocean surface current and this phenomenon must be reflected in the electromagnetic backscattering signals. To find the effect of ocean current on the electromagnetic backscattering of the fractal sea surface, the above parameters in this section are applied to our electromagnetic backscattering model to simulate the electromagnetic backscattering signals from the 1D drifting fractal sea surface. As an example, the ocean current velocities range from -1.5 m·s^{-1} to 1.5 m·s^{-1} in steps of 0.5 m·s^{-1} in our simulations. The NRCS's of these wave–current effects in the coupled sea surface model, with incidence angles ranging from 0° to 70°, are shown in Fig. 3.

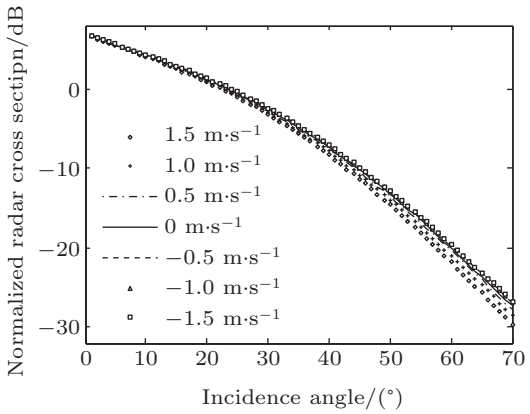


Fig. 3. NRCS's due to wave–current interactions in the coupled sea surface model with incidence angles ranging from 0° to 70°, where current velocities are $C_0 = -1.5$ m·s^{-1}, -1.0 m·s^{-1}, -0.5 m·s^{-1}, 0 m·s^{-1}, 0.5 m·s^{-1}, 1.0 m·s^{-1}, and 1.5 m·s^{-1}, respectively.

Figure 3 shows that the NRCS decreases with increasing incidence angle for backscattering from the fractal sea surface with different ocean current velocities. This result is consistent with the previous conclusion based on both theoretical results and observations. The effects of ocean current on electromagnetic backscattering of the fractal sea surface can also be found in Fig. 3. The solid line shows the NRCS of uncoupled fractal sea surface varying with incidence angle. The NRCS of the coupled wave–current fractal sea surface is larger than that of the uncoupled fractal sea surface when the current velocity is given by $C_0 < 0$ m·s^{-1}, and vice versa. Therefore, ocean currents can enhance the NRCS of the fractal sea surface when the wave propagates in the opposing direction to the current propagation direction, whereas the NRCS of the fractal sea surface is weakened by the currents travelling in the same direction as the wave propagation direction.

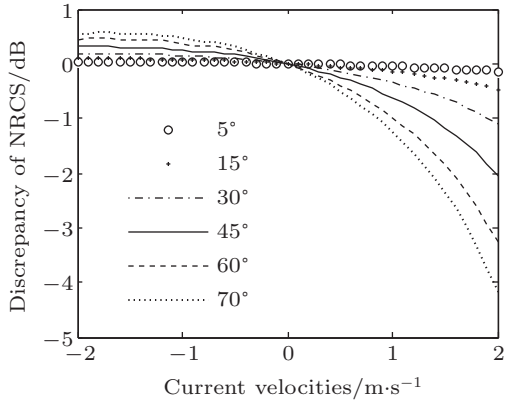


Fig. 4. Discrepancies of NRCS, caused by ocean currents at incidence angles of 5°, 15°, 30°, 45°, 60°, and 70°.

To show the details of the effects of ocean currents on electromagnetic backscattering of the fractal sea surface, dis-

crepancies of the NRCS ($\Delta\sigma_0$) between the coupled wave–current fractal sea surface model and the uncoupled fractal sea surface model are shown in Fig. 4. Note that it is easier to find the effects of ocean currents on electromagnetic backscattering of the fractal sea surface in Fig. 4 than the analogous results in Fig. 3. From Fig. 4, one can obtain several results.

Firstly, the discrepancies of NRCS ($|\Delta\sigma_0|$) increase with increasing current velocity ($|C_0|$) when waves propagate in the direction opposite to or the same as the current propagation direction. This result can also be found in Table 1. For example, $\Delta\sigma_0 = 0$ when $C_0 = 0$ and incidence angle is 5°. $|\Delta\sigma_0|$ changes gradually from 0 to 0.15 dB when C_0 increases from 0 to 2.0 m·s^{-1}. On the other hand, $\Delta\sigma_0$ changes gradually from 0 to 0.05 dB when C_0 changes from 0 to -2.0 m·s^{-1}, i.e., $|C_0|$ increases from 0 to 2.0 m·s^{-1}.

Table 1. Discrepancies of NRCS ($\Delta\sigma_0$) between the coupled wave–current fractal sea surface model and the uncoupled fractal sea surface model.

θ	$\Delta\sigma_0$/dB								
	–2	–1.5	–1	–0.5	0	0.5	1	1.5	2[a]
5°	0.05	0.04	0.03	0.02	0	–0.03	–0.07	–0.11	–0.15
15°	0.11	0.09	0.08	0.05	0	–0.06	–0.17	–0.29	–0.47
30°	0.21	0.19	0.15	0.11	0	–0.15	–0.35	–0.65	–1. 21
45°	0.33	0.31	0.25	0.16	0	–0.27	–0.63	–1.17	–2.05
60°	0.45	0.44	0.39	0.25	0	–0.41	–1.0	–1.87	–3.29
70°	0.55	0.54	0.47	0.31	0	–0.53	–1.25	–2.37	–5.19

[a]C_0 in units of m·s^{-1}.

Secondly, the effect of ocean current on electromagnetic backscattering from the fractal sea surface when $C_0 < 0$ m·s^{-1} is less than that of ocean current with $C_0 > 0$ m·s^{-1}. The case of incidence angle 70° in Table 1 can be used to provide quantitative analysis of this result. We select $|C_0| = 2$ m·s^{-1} here. The result in Table 1 shows that $|\Delta\sigma_0| = 0.55$ dB when $C_0 = -2$ m·s^{-1} while $|\Delta\sigma_0| = 419$ dB when $C_0 = -2$ m·s^{-1}. The latter $|\Delta\sigma_0|$ is 7.6 times the former $|\Delta\sigma_0|$. Similar results can be obtained when comparing the values of $|\Delta\sigma_0|$ in the cases of C_0 and $-C_0$.

Thirdly, the discrepancy in NRCS ($|\Delta\sigma_0|$) between the coupled wave–current fractal sea surface model and the uncoupled fractal sea surface model increases with increasing incidence angle. This point is also shown in Table 1. As an example, for the selected ocean current -1.5 m·s^{-1}, $|\Delta\sigma_0|$ increases from 0.04 dB to 0.54 dB when the incidence angle increases from 5° to 70° .

4. Conclusions

Ocean current patterns are typically found in SAR images, especially those covering strong currents, such as the Gulf Stream. Thus far, there have been no established methods to retrieve ocean currents by remote sensing technology. In order to solve this problem, the EM backscattering mechanism of coupled wave–current interactions on the sea surface should be studied in depth.

Our work concentrates on establishing an EM scattering model for the 1D drifting fractal sea surface, and then studying the modulation characteristics of surface currents on the EM backscattering signals. The coupled wave–current fractal sea surface model is derived based on the wave–current interaction mechanism investigated in Part 1 of our work.[20] Based on the wave–current coupled model presented in Part 1, the 1D electromagnetic backscattering model of the wave–current fractal sea surface is derived in this paper.

Applying our electromagnetic backscattering model, numerical results show that both the magnitude and the direction of ocean current have influences on the EM backscattering signals from the 1D coupled wave–current fractal sea surface. Therefore, ocean currents which are parallel to the propagation direction of the wave can weaken the EM backscatter signal intensity. By comparison, the EM backscattering signal intensity can be strengthened by ocean current propagating in the opposing direction to the wave propagation direction. Furthermore, the effect of ocean current on the 1D fractal sea surface grows as the ocean current velocity increases. Finally, the discrepancy in the NRCS ($\Delta\sigma_0$) between the coupled wave–current fractal sea surface model and the uncoupled fractal sea surface model increases with increasing incidence angle.

In future, our electromagnetic backscattering model for the 1D drifting fractal sea surface can be applied to study the SAR imaging mechanism of the drifting sea surface. This methodology may be one of the effective methods to explore new methods to retrieve ocean currents from SAR images.

References

[1] Dugan J P and Piotrowski C C 2003 *Remote Sens. Env.* **84** 309
[2] Dugan J P and Piotrowski C C 2012 *J. Geophys. Res.* **117** C03020
[3] Brrick D E, Evans M W and Weber B L 1977 *Science* **198** 138
[4] Chapman R D, Shay L K, Graber H C, Edson J B, Karachintsev A, Trump C L and Ross D B 1997 *J. Geophys. Res.* **102** 18737
[5] Paduan J D and Shulman I 2004 *J. Geophys. Res.* **109** C07S09
[6] Abascal A J, Castanedo S, Fernandez V and Medina R 2012 *Ocean Dyn.* **62** 1073
[7] Paduan J D and Washburn L 2013 *Annu. Review Mari. Sci.* **5** 115
[8] Ullman D S, O'Donnell J, Kohut J, Fake T and Allen A 2006 *J. Geophys. Res.* **111** C12005
[9] Lorente P, Piedracoba S and Alvarez-Fanjul E 2015 *Cont. Shelf Res.* **92** 1
[10] de MicheleM, Leprince S, Thiebot J, Raucoules D and Binet R 2012 *Remote Sens. Env.* **11** 9266
[11] Piotrowski C C and Dugan J P 2002 *IEEE Trans. Geosci. Remote Sens.* **40** 2606
[12] Dugan J P, Anderson P P, Piotrowski C C and Zuckerman S B 2014 *IEEE Trans. Geosci. Remote Sens.* **52** 3895
[13] Shuchman R A, Lyzenga D R and Klooster A 1981 *Exploitation of SAR Data for Measurement of Ocean Currents and Wave Velocities,* Report (NASA) A1
[14] Chapron B, Collard F and Ardhum F 2005 *J. Geophys. Res.* **110** C07008

[15] Kudryavtsev V, Akimov D, Johannessen J A and Chapron B 2005 *J. Geophys. Res.* **110** C07016
[16] Johannessen J A, Chapron B, Collard F, Kudryavtsev V, Mouche A, Akimov D and Dagestad K F 2008 *Geophys. Res. Lett.* **35** L22608
[17] Goldstein R M and Zebker H A 1987 *Nature* **328** 707
[18] Romeiser R 2005 *IEEE J. Ocean Eng.* **30** 552
[19] Romeiser R, Runge H, Suchandt S, Sprenger J, Weilbeer H, Sohrmann A and Stammer D 2007 *IEEE Trans. Geosci. Remote Sens.* **45** 4019
[20] Xie T, Fang H, Zhao S, Yu W and He Y 2016 *Chin. Phys. B* **25** 064101
[21] Leung T, Kong J and Robert T 1985 *Theory of Microwave Remote Sending* (New York: Wiley) p. 70